Tumor Control Probability and Small-Scale Monte Carlo Dosimetry: Effects of Heterogenous Intratumoral Activity Distribution in Radiopharmaceutical Therapy

Emma Mellhammar[1], Magnus Dahlbom[2], Oskar Vilhelmsson-Timmermand[1,3], and Sven-Erik Strand[1,4]

[1]Oncology, Department of Clinical Sciences Lund, Lund University, Lund, Sweden; [2]Department of Molecular and Medical Pharmacology, David Geffen School of Medicine, UCLA, Los Angeles, California; [3]Imaging Chemistry and Biology, King's College London, London, United Kingdom; and [4]Medical Radiation Physics, Department of Clinical Sciences Lund, Lund University, Lund, Sweden

In radiopharmaceutical therapy, intratumoral uptake of radioactivity usually leads to heterogeneous absorbed dose distribution. The likelihood of treatment success can be estimated with the tumor control probability (TCP), which requires accurate dosimetry, estimating the absorbed dose rate per unit activity to individual tumor cells. **Methods:** Xenograft cryosections of the prostate cancer cell line LNCaP treated with [^{177}Lu]Lu-PSMA-617 were evaluated with digital autoradiography and stained with hematoxylin and eosin. The digital autoradiography images were used to define the source in a Monte Carlo simulation of the absorbed dose, and the stained sections were used to detect the position of cell nuclei to relate the intratumoral absorbed dose heterogeneity to the cell density. Simulations were performed for ^{225}Ac, ^{177}Lu, and ^{90}Y. TCP was calculated to estimate the mean necessary injected activity for a high TCP. A hypothetical case of activity mainly taken up on the tumor borders was generated and used to simulate the absorbed dose. **Results:** The absorbed dose per decay to tumor cells was calculated from the staining and simulation results to avoid underestimating the tumor response from low absorbed doses in tumor regions with low cell density. The mean of necessary injected activity to reach a 90% TCP for ^{225}Ac, ^{177}Lu, and ^{90}Y was found to be 18.3 kBq (range, 18–22 kBq), 24.3 MBq (range, 20–29 MBq), and 5.6 MBq (range, 5–6 MBq), respectively. **Conclusion:** To account for the heterogeneous absorbed dose generated from nonuniform intratumoral activity uptake, dosimetry models can estimate the mean necessary activity to reach a sufficient TCP for treatment response. This approach is necessary to accurately evaluate the efficacy of suggested radiopharmaceuticals for therapy.

Key Words: Monte Carlo dosimetry simulation; radiopharmaceutical therapy; digital autoradiography; tumor control probability; heterogeneity

J Nucl Med 2023; 64:1632–1637
DOI: 10.2967/jnumed.123.265523

Radiopharmaceutical therapy has become a promising approach to treating metastatic cancers, such as metastatic castrate-resistant prostate cancer (*1,2*). Radiopharmaceuticals that target cell-specific epitopes emitting short-range radiation with high linear energy transfer can deliver high absorbed doses to tumors while sparing healthy tissues. Nonuniform uptake of radiopharmaceuticals in a targeted volume can cause heterogeneous energy depositions, leading to large variations in the absorbed dose experienced by the cells.

The MIRD formalism assumes uniform activity in the source and calculates an average absorbed dose to the target volumes (*3,4*). Although the formalism can be applied on any scale, macroscopic or microscopic, it is commonly used with data from γ-cameras or SPECT imaging, where spatial resolution and sensitivity are limited and mainly organs can be delineated. Instead, digital autoradiography (DAR) can detect the intratumoral distribution of radioactivity (*5–8*). Chouin et al. used an α-camera to estimate the absorbed dose to cells in micrometastases after treatment with a radioimmunoconjugate labeled with ^{211}At (*9*). Similar to the study presented here, they correlated the detected activity in cryosections to cells detected in adjacent sections stained with hematoxylin and eosin (HE).

Detailed dosimetry models in preclinical trials can help identify the most promising tracers for radiopharmaceutical therapy. Unexplained failure of tracers could be resolved by improving the tumor penetration of the tracer, optimizing for more homogeneous intratumoral distribution of the tracer, or changing the labeled radionuclide to one with longer-range emission. Our group previously improved the tumor uptake uniformity of ^{111}In-DOTA-hu5A10 by increasing the chelate-to-antibody molar ratio in the labeling process, thereby improving the therapeutic effect in treated xenografted mice (*10*). Similarly, Howe et al. showed that a combination of carriers labeled with ^{225}Ac with complementary intratumoral distributions generated improved radioactivity distribution and significantly reduced tumor growth compared with the same activity delivered by either of the 2 carriers alone (*11*).

The tumor control probability (TCP) estimates the probability of killing all cells in a lesion from absorbed dose and cell radiosensitivity data (*12–14*). The intratumoral radioactivity distribution affects TCP for short-range radiation (*15*). This paper aims to calculate TCP from dosimetry simulations of heterogeneous activity distributions measured with DAR.

Received Jan. 30, 2023; revision accepted Jun. 12, 2023.

For correspondence or reprints, contact Emma Mellhammar (emma.mellhammar@med.lu.se).

Published online Jul. 27, 2023.

MATERIALS AND METHODS

Sections from xenografts treated with [^{177}Lu]Lu-PSMA-617 from BALB/cAnNRj mice were used to build a dosimetry model. The activity detected in the DAR image pixels was used to define voxels in the source volume in a Monte Carlo simulation of the absorbed dose. By matching DAR and HE images, the cells segmented from the HE stain within an aligned DAR image pixel were assumed to receive the absorbed dose simulated to the corresponding target voxel. TCP, as a function of injected activity, was calculated considering the cell's simulated absorbed dose per decay (from now on called dose values or dose image). Detailed descriptions of radiolabeling, cell culturing, animal work, and autoradiography can be found in supplemental materials (supplemental materials are available at http://jnm.snmjournals.org).

Monte Carlo dose simulations of ^{177}Lu, ^{90}Y, and ^{225}Ac were performed in GATE version 8.1 (OpenGATE), which in turn uses Geant4 version 10.3.3 (European Organization for Nuclear Research) (*16*). All image and data processing were performed in MATLAB R2020b (MathWorks). Each tumor's 8 DAR images were decay-corrected to the same time point and aligned (coregistered), an average of the images was calculated, and grayscale values were normalized. The tumor borders were detected by thresholding the grayscale values. The resulting mask was used to coregister the DAR and HE images. Cell nuclei were segmented from the HE images (details in supplemental materials), and a cell density map was generated in which the number of cells within the corresponding pixel in the coregistered DAR image was calculated. A hypothetical case in which the activity is primarily taken up at the edge of the xenograft because of low tumor penetration was generated by filtering the mean DAR images (description and filter in Supplemental Fig. 1).

GATE Monte Carlo Simulations

The β-decay of both ^{177}Lu and ^{90}Y has a yield of 100%, and the primary β-emissions were included in the simulations. ^{177}Lu emits β-particles with maximum (endpoint) β energy ($E_{β(max)}$) of 497 keV (79.4%), 384 keV (8.9%), 247 keV (0.016%), and 176 keV (11.7%) (*17*). ^{90}Y emits β-particles with $E_{β(max)}$ of 2,279 keV (99.9%), 518 keV (0.01%), and 92 keV (0.0000014%) (*17*). The mean β-energy spectrums of these emissions considered for ^{177}Lu and ^{90}Y, shown in Supplemental Figure 2A, were collected from the International Atomic Energy Agency's Livechart of Nuclides (*17*)—originally computed by Betashape (*18,19*)—and defined in GATE as histogram sources. The histogram had a step width of 0.5 keV for ^{177}Lu and 0.3 keV for ^{90}Y. No other electron or γ-emissions were considered because it was assumed their contribution to the final absorbed dose was negligible.

For ^{225}Ac simulations, the highest-energy α-emission of 5.8 MeV was considered, together with the highest-energy α-emissions from the daughters ^{221}Fr (6.4 MeV), ^{217}At (7.1 MeV), and ^{213}Po (8.4 MeV), thereby simplifying and speeding up the simulation. The decay chain of ^{225}Ac is shown in Supplemental Figure 2B. The daughters were assumed to remain immobile relative to the mother nuclide. To generate a realistic distribution of these emissions, a discrete spectrum was defined in the GATE simulation, where the 4 α-energies all have the same probability of being emitted as primary particles. Again, no γ-particles or electrons were included in this simulation because they were assumed to be negligible.

In the simulation, the world was defined as a water cube. To build a source volume, each pixel of the mean DAR image was defined as a box-shaped, general-purpose source placed in the water volume as a grid of voxels. The energy spectrum of the simulated radionuclide was ascribed to the general-purpose sources. The intensity of each source voxel was set to the normalized grayscale pixel values of the mean DAR image, thereby giving the relative probability for the emission of a simulated particle. Their *x*- and *y*-dimensions remained 50 × 50 μm, like the DAR image pixel size. The *z*-dimension was set to twice the continuous slowing-down approximation range in liquid water of the maximum energy of the emission of the radionuclide, except for ^{90}Y. Instead, the range was limited to 10 mm, because no axis length of the included tumors was longer. For ^{225}Ac, the daughter ^{213}Po had the highest α-energy considered in the simulation, with an estimated continuous slowing-down approximation range of 0.085 mm (*20*). For ^{177}Lu, the $E_{β(max)}$ 496.8 MeV equated to a continuous slowing-down approximation range of 1.8 mm (*20*). The electromagnetic interactions of the primary and secondary emissions were simulated by the Geant4 physics list emstandard_opt3 (*16*).

The energy of simulated primary particles was sampled from the energy spectrum, and its origin was sampled from the voxel intensities. Simulations were run for 10^9 primary particle emissions. A GATE dose actor was defined that overlapped the source voxel volume with the same resolution as the source in the *x*- and *y*-direction ($50 \times 50\ \mu m^2$) and 10 μm in the *z*-direction, mimicking the tumor cryosection thickness. To convert the absorbed dose recorded in the target volume to the absorbed dose per decay (Gy $Bq^{-1}\ s^{-1}$), S_i in the *i*th voxel was calculated as the total number of nuclear transformations (decays), and the simulated absorbed dose was multiplied with the yield *Y* of the emissions and the number of primary particle emissions *P* in the simulation (Equation 1):

$$S_i = D_{\mathrm{sim},i} \cdot \frac{Y}{P}. \quad \text{Eq. 1}$$

For ^{177}Lu and ^{90}Y, the yield *Y* equals 100%. For ^{225}Ac, the α-decay has a 100% yield. However, because of the included daughter α-emissions, 1 in 4 of the simulated primary particles originate from ^{225}Ac; therefore, the ^{225}Ac yield in the simulation can be described as 400%.

The cell density map was used to overlap the resulting simulated dose image. Cells detected in the corresponding target voxel were assumed to receive its absorbed dose per decay. Histograms of equal binning of target voxels and cell dose values were used to calculate the cumulated dose–volume histograms.

TCP, as a function of injected activity, was calculated from the cell dose values. For each dose value interval *j,* the absorbed dose D_j was calculated. It is defined by the MIRD formalism (*3*) as the product of the cumulated activity $\tilde{A}$ and the dose value:

$$D_j = \tilde{A} \cdot S_j = \frac{T_{1/2}}{\ln(2)} \cdot A_0 \cdot S_j. \quad \text{Eq. 2}$$

where $T_{1/2}$ is the physical half-life.

The initial activity A_0 in the source volume was calculated as the product of the uptake *U* (percentage injected activity per gram), assuming instantaneous uptake; the injected activity A_{inj} (Bq); and the tumor source volume considered in the simulation V_{source} (g):

$$A_0 = U \cdot V_{\mathrm{source}} \cdot A_{\mathrm{inj}}. \quad \text{Eq. 3}$$

To exemplify a realistic case, average activity uptake was assumed to be 3.6% per injected activity per gram of xenograft tissue, as previously measured by our group (*22*), with a tissue density of 1.0 g/cm^3.

The cumulated activity is the total number of decays from the fraction of the injected activity taken up by the tumor. To exemplify the use of DAR images for TCP calculations, we simplified the model. We assumed no biologic clearance and no redistribution within the tumor. All activity measured 3 d after injection was therefore assumed to have been taken up instantaneously without redistribution during the dose integration period. For a more realistic model, uptake should be measured at several time points to estimate the cumulated activity better. For each radionuclide, a range of injected activities was evaluated within relevant intervals; 0–100 MBq for ^{177}Lu, 0–30 MBq for ^{90}Y, and 0–100 kBq for ^{225}Ac.

The survival probability and TCP were calculated as previously described by Nahum (*13*) and Bernhardt et al. (*12*) and later summarized by Uusijärvi et al. (*14*). For each dose value interval *j,* the survival probability SP_j for the cells in that interval that were assumed to be identical was calculated as in Equation 1. A range of values for the radiosensitivity α in a relevant interval based on radiosensitivity measurements performed by Elgqvist et al. (*21*) was applied in the calculations to evaluate its effect on the resulting TCP:

$$SP_j = e^{-(\alpha \times D_j)}. \qquad \text{Eq. 4}$$

Equation 4 is a simplification of the linear-quadratic model (*13*) and is applicable for radiation with high linear energy transfer, such as α-particles or β-particles delivering an absorbed dose of more than approximately 2 Gy.

TCP, defined as the probability to kill all cells, for all intervals *j*—normalized for the number of cells N_c in each interval receiving the absorbed dose D_j—is then given by the following equation:

$$\text{TCP} = \prod_{j=1}^{N_c} (1 - SP_j). \qquad \text{Eq. 5}$$

RESULTS

The results for tumor 3 are presented here. Results for tumors 1 and 2 are found in Supplemental Figures 3–25.

The mean of 8 aligned DAR images from tumor 3 is shown in Figure 1A. The modified DAR image, shown in Figure 1B, represents a case of reduced tumor penetration. Activity has been moved from the central parts of the tumor and concentrated on the edges. The cell density map of tumor 3 in Figure 1C found between 0 and 30 cells per pixel. Segmentation results are presented in Supplemental Table 1.

The resulting dose values in the dose actor voxels in tumor 3 are presented in Figure 2. The differing particle range of the 3 radionuclide emissions can be seen in the gradually smoother distribution as the range increases. The long range of the ^{90}Y β-particles generated a smooth dose image in which local variations in activity uptake were indistinguishable. In contrast, the α-particle emissions of ^{225}Ac and its daughters caused a more heterogeneous distribution with hot spots induced by local activity clusters. Effectively, cells residing in a voxel with low activity uptake could still receive a relatively high dose value when simulations were run for ^{90}Y but depended more on local uptake when ^{225}Ac was simulated. Similar results were seen for tumors 1 and 2 (Supplemental Fig. 4).

For simulations performed with the modified activity distributions, the maximum dose values for all radionuclides increased, as did the focus of higher dose values to voxels with higher source intensity. Although ^{90}Y generated the most homogeneous dose value distribution, differences between edges and central parts increased (Supplemental Fig. 5).

The cell dose value distribution, calculated by matching the dose value image to the cell density map, for ^{177}Lu in tumor 3 is presented in the histogram in Figure 3A. Although the mean absorbed dose rate per unit activity in cells was 2.2×10^{-10} Gy Bq^{-1} s^{-1}, it ranged from close to 0 to more than 4×10^{-10} Gy Bq^{-1} s^{-1}. This can be compared with the target voxel dose value distribution shown in Figure 3B, where the mean was 1.2×10^{-10} Gy Bq^{-1} s^{-1}. The shape of the histograms differs greatly, because the cell density varies over the tumor section. Many voxels experienced a low dose value, but these contained few cells, whereas the cell dose value distribution was approximately centered on its mean. The cumulated absorbed dose rate histograms for cells and voxels are plotted in Figure 3C.

The resulting cell dose value histograms of all tumors and radionuclides are shown in Supplemental Figure 15, and the modified activity distributions appear in Supplemental Figure 16. Comparing ^{90}Y and ^{177}Lu, the mean absorbed dose rate per unit activity was higher for ^{90}Y. However, between the two, the highest dose value was received by ^{177}Lu in tumor 2.

From the cell dose value histograms, TCP was calculated for all 3 tumors as a function of injected activity for ranges of activity realistic to inject in a mouse model. Elgqvist et al. investigated the radiosensitivity of several prostate cancer cell lines, including LNCaP (*21*). By fitting their data to Equation 4, LNCaP should have a radiosensitivity of 1.33 Gy^{-1} (95% CI, 0.96–1.70 Gy^{-1}) for α-particles and 0.21 Gy^{-1} (95% CI, 0.16–0.25 Gy^{-1}) for β-particles. Based on this, TCP was calculated as in Equation 5 for intervals of radiosensitivity of 0.5, 1.0, 1.3, and 2.0 Gy^{-1} for ^{225}Ac and 0.1, 0.2, 0.3, and 0.4 Gy^{-1} for ^{177}Lu and ^{90}Y. The resulting TCPs for tumor 3 are shown in Figure 4. Corresponding figures for tumors 1 and 2 can be found in Supplemental Figures 17–25. The necessary activities to be injected to reach a 90% TCP are summarized in Table 1, and the modified activity distributions are summarized in Table 2.

When treating tumor 3 with ^{225}Ac, as shown in Figure 4A, an injection of about 20–30 kBq should be expected to give a good tumor response. However, when the activity remained at the border of the tumor, as shown in Figure 1B, the injected activity needed to reach a 90% TCP greatly increased, as seen in Table 2. This TCP level was never reached for a radiosensitivity of 0.5 Gy^{-1}; however, this was a low estimate for radiosensitivity. The necessary activities to be injected might be so high that they cause damage to healthy tissues.

For treatment of tumor 3 with ^{177}Lu, as shown in Figure 4B, an injection of less than 30 MBq would unlikely be curative. The necessary activity for a high TCP increased when the activity distribution in the tumor was modified, as summarized in Table 2. For a radiosensitivity of 0.1 Gy^{-1}, no activity below 100 MBq was sufficient to reach a 90% TCP.

Finally, TCP for tumor 3 treated with ^{90}Y is shown in Figure 4C. The relative difference in activity needed for a 90% TCP when comparing the original and the modified activity distribution is smaller for ^{90}Y than for ^{177}Lu and ^{225}Ac because of its longer β-particle range.

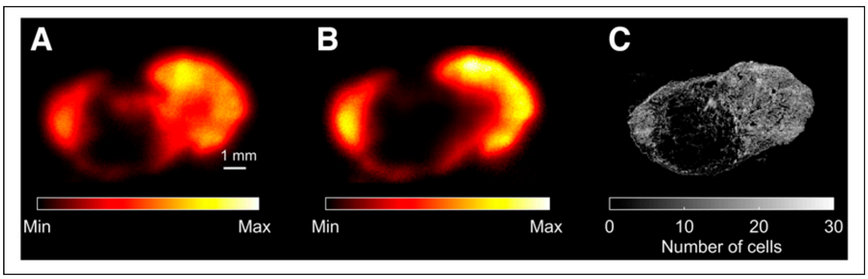

FIGURE 1. Mean DAR image (A), modified DAR image after filtering (B), and cell density map (C) for tumor 3. (A) Mean DAR image results from averaging 8 DAR sections after coregistration. (B) Hypothetical case of reduced tumor penetration. (C) Number of cells in corresponding target voxels in simulation.

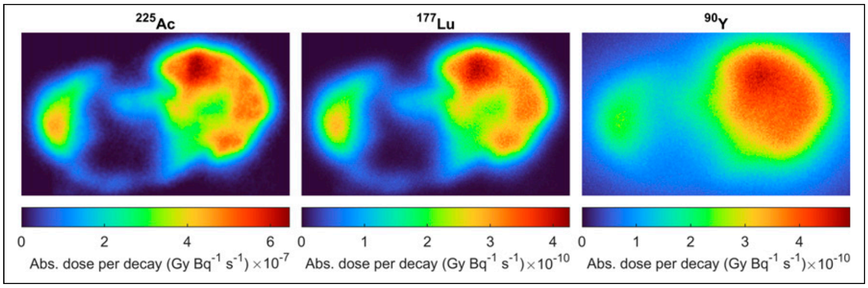

FIGURE 2. Simulated absorbed dose per unit activity in LNCaP tumor cryosections from tumor 3 for α- or β-emissions of ^{225}Ac, ^{177}Lu, and ^{90}Y. Abs. = absorbed.

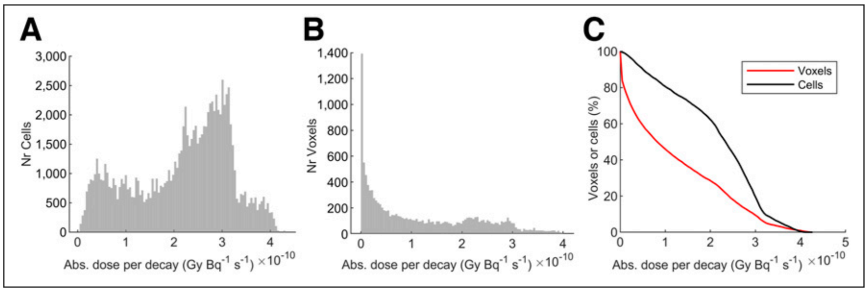

FIGURE 3. Cell dose value distribution for tumor 3 when treated with ^{177}Lu (A), compared with voxel dose value distribution (B), and cumulated dose–volume histograms of dose values for either cells or voxels (C). Abs. = absorbed; Nr = number.

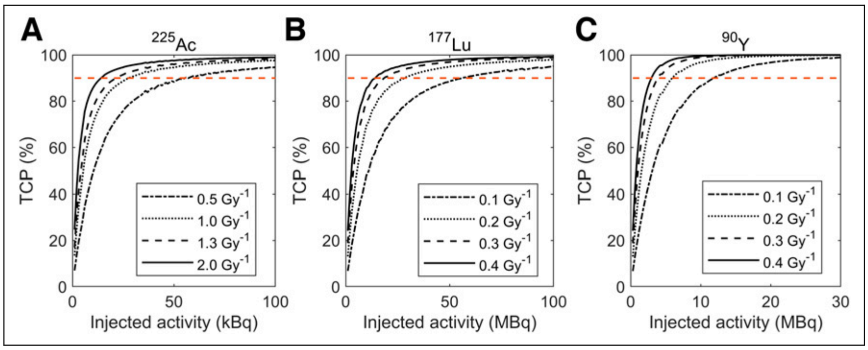

FIGURE 4. TCP vs. injected activity in tumor 3 investigated for radiosensitivities of 0.5–2.0 Gy^{-1} for ^{225}Ac (A) and 0.1–04 Gy^{-1} for ^{177}Lu (B) and ^{90}Y (C). Dashed line indicates 90% TCP level.

For comparison, if TCP was instead calculated from the voxel dose values, none of the investigated injected activities or radiosensitivities reached a TCP of at least 90% for ^{225}Ac or ^{177}Lu in tumor 3 (results in Supplemental Figs. 17, 20, and 23).

DISCUSSION

A common approach for tumor dosimetry in radiopharmaceutical therapy is to assume a sphere or ellipsoid of evenly distributed tumor cells with homogeneous radioactivity uptake. For short-range radiation, this oversimplification is inappropriate (*23*), because it risks miscalculating the absorbed dose to cells if activity uptake is heterogeneous. This is accounted for by performing voxel dosimetry, which still ignores the cellular distribution.

In preclinical trials, dosimetry models are necessary to evaluate which radiotracers have the potential to generate good treatment responses. However, overly simplified dosimetry models might mislead researchers instead of guiding their decision-making. An improvement considers intratumoral activity uptake and its relation to tumor cell distribution. Then, based on TCP calculations, realistic activities to be injected for optimal treatment effect can be estimated.

This study simulates heterogeneous absorbed dose distributions within xenografts treated with PSMA-617–ligated radioactivity. To improve calculations of TCP, we connect dose values to the number of cells experiencing them. This generates a dose value distribution that is different from the distribution generated when only voxels are considered, as seen in Figures 3A and 3B. This way, the treatment response to a wasted dose—that is, energy deposited in volumes where few cells reside—and the response of cells in volumes receiving less than necessary for tumor control will not be overestimated.

We estimate the minimum injected activities necessary to reach a 90% TCP for varying radiosensitivities. For ^{225}Ac, assuming a radiosensitivity of 1.3 Gy^{-1}, the mean injected activity would be 18.3 kBq (range, 18–22 kBq). For ^{177}Lu and ^{90}Y, assuming a radiosensitivity of 0.2 Gy^{-1}, a mean of 24.3 MBq (range, 20–29 MBq) and 5.6 MBq (range, 5–6 MBq), respectively, would

TABLE 1
Injected Activity of ^{225}Ac, ^{177}Lu, or ^{90}Y Necessary to Reach TCP of 90%

Radioactivity	^{225}Ac (kBq)				^{177}Lu (MBq)				^{90}Y (MBq)			
Radiosensitivity (Gy^{-1})	0.5	1.0	1.3	2.0	0.1	0.2	0.3	0.4	0.1	0.2	0.3	0.4
Tumor 1	39	20	15	10	40	20	13	10	9.5	5	3.5	2.5
Tumor 2	47	24	18	12	47	24	16	12	12	6	4	3
Tumor 3	55	28	22	14	56	29	19	14	12	6	4.5	3

Calculations were made for ranges of radiosensitivity of 0.5, 1.0, 1.3, and 2.0 Gy^{-1} for ^{225}Ac and 0.1, 0.2, 0.3, and 0.4 Gy^{-1} for ^{177}Lu and ^{90}Y.

TABLE 2
Injected Activity of ^{225}Ac, ^{177}Lu, or ^{90}Y Necessary to Reach TCP of 90% for Modified Activity Distribution

Radioactivity	^{225}Ac (kBq)				^{177}Lu (MBq)				^{90}Y (MBq)			
Radiosensitivity (Gy^{-1})	0.5	1.0	1.3	2.0	0.1	0.2	0.3	0.4	0.1	0.2	0.3	0.4
Tumor 1	—	90	34	29	78	39	26	20	11	6	4	3
Tumor 2	—	80	31	27	66	35	23	18	12	6	4	3
Tumor 3	—	86	66	42	—	77	52	39	14.5	7.5	5	4

Calculations were made for ranges of radiosensitivity of 0.5, 1.0, 1.3, and 2.0 Gy^{-1} for ^{225}Ac and 0.1, 0.2, 0.3, and 0.4 Gy^{-1} for ^{177}Lu and ^{90}Y.

be necessary. In the case of ^{177}Lu, these numbers agree with the injected activities that resulted in good tumor response when previously investigated by our group (*22*). The sample consists of only 3 tumors, so the resulting numbers are uncertain.

Along the slicing axis of the sectioned xenograft, the activity distribution and cell density change only slightly. This is an argument for the validity of our approach to evaluating the TCP of the tumor, because we assume the TCP of a section of the tumor is representative of the whole tumor.

We present here a general model; more parameters should be included to increase the accuracy. In our model, uptake is based on a single time point, and there is a lack of pharmacokinetics because we have included only the physical clearance of the radionuclides. Some biologic clearance is expected, so the results likely overestimate TCP. By measuring at several time points, one might improve the estimate of cumulated activity. In addition, no consideration of DNA damage repair, tumor repopulation, or differences in dose rate, which are relevant (*24*), is made.

Regions of varying cell density and cell type, necrotic areas, vascular structures, etc., are seen throughout the tumor volumes. In addition, the targeted epitopes of the tumor cells might not be equally available because of restricted tumor penetration or varying expression. Bordes et al. (*25*) used the measured uptake of rituximab by fluorescence microscopy in a multicellular aggregate of lymphoma cells, distinctly limited to the edges, to represent activity uptake in Monte Carlo simulations of the absorbed dose rate per activity unit in multicellular volumes (*25*). This method is favored by the greater resolution of fluorescence microscopy. However, it is not a direct measurement of actual activity uptake, because uptake might differ when labeling a tracer molecule to a radionuclide rather than a fluorophore.

For short-range radiation with high linear energy transfer, the microscopic energy deposition distribution can affect the absorbed dose to the cell nucleus. Cellular internalization can shorten the distance between decay and nucleus, thereby increasing energy deposited where it is most effective. The DAR images' pixel size limits the spatial resolution. Similar to the range of α-particles emitted in the ^{225}Ac decay chain, no microscale heterogeneity will be considered. However, Mínguez Gabiña et al. simulated TCP in a cluster of cells with varying ^{225}Ac-PSMA internal uptake and only found a small difference between activity on the cell surface and activity inside the cytoplasm (*26*).

CONCLUSION

We have shown how to improve preclinical dosimetry in radiopharmaceutical therapy by considering intratumoral activity uptake and its relation to tumor cell distributions. Realistic activities to be injected for optimal treatment effect can be determined with Monte Carlo simulations and TCP calculations. Examples are given for LNCaP xenografts treated with radiolabeled PSMA-617. Our approach, which considers the intratumoral distribution of cells rather than only the voxel volume, avoids underestimating the mean experienced absorbed dose rate per unit activity, because the influence of the wasted dose on the dose value calculations is reduced.

DISCLOSURE

This study was performed with support from the Swedish Cancer Society and Mrs. Berta Kamprad's Foundation. No other potential conflict of interest relevant to this article was reported.

ACKNOWLEDGMENTS

We thank Wahed Zedan for cell culturing and animal handling and Anders Örbom for help with DAR imaging.

KEY POINTS

QUESTION: Can combining DAR images with HE-stained xenograft sections in a Monte Carlo dosimetry model improve calculations of TCP?

PERTINENT FINDINGS: The model finds dose values experienced by cells in the tumor. We calculated TCP and estimated the necessary injected activity for LNCaP xenografts treated with PSMA-617 radiolabeled to ^{225}Ac, ^{177}Lu, and ^{90}Y.

IMPLICATIONS FOR PATIENT CARE: Improved dosimetry models are vital to evaluate radiotracers' potential in a preclinical phase.

REFERENCES

1. Fendler WP, Rahbar K, Herrmann K, Kratochwil C, Eiber M. ^{177}Lu-PSMA radioligand therapy for prostate cancer. *J Nucl Med.* 2017;58:1196–1200.
2. Kratochwil C, Bruchertseifer F, Giesel FL, et al. ^{225}Ac-PSMA-617 for PSMA-targeted alpha-radiation therapy of metastatic castration-resistant prostate cancer. *J Nucl Med.* 2016;57:1941–1944.
3. Bolch WE, Eckerman KF, Sgouros G, Thomas SR. MIRD pamphlet no. 21: a generalized schema for radiopharmaceutical dosimetry—standardization of nomenclature. *J Nucl Med.* 2009;50:477–484.
4. Sgouros G, Dewaraja YK, Escorcia F, et al. Tumor response to radiopharmaceutical therapies: the knowns and the unknowns. *J Nucl Med.* 2021;62(suppl 3):S12–S22.

5. Örbom A, Miller BW, Bäck T. Beta and alpha particle autoradiography. In: Ljungberg M, ed. *Handbook of Nuclear Medicine and Molecular Imaging for Physicists: Instrumentation and Imaging Procedures.* CRC Press/Balkema; 2021: 563–587.
6. Ljunggren K, Strand SE. Beta camera for static and dynamic imaging of charged-particle emitting radionuclides in biologic samples. *J Nucl Med.* 1990;31:2058–2063.
7. Bäck T, Jacobsson L. The alpha-camera: a quantitative digital autoradiography technique using a charge-coupled device for ex vivo high-resolution bioimaging of alpha-particles. *J Nucl Med.* 2010;51:1616–1623.
8. Örbom A, Ahlstedt J, Serén T, et al. Characterization of a double-sided silicon strip detector autoradiography system. *Med Phys.* 2015;42:575–584.
9. Chouin N, Lindegren S, Frost SH, et al. Ex vivo activity quantification in micrometastases at the cellular scale using the alpha-camera technique. *J Nucl Med.* 2013; 54:1347–1353.
10. Vilhelmsson Timmermand O, Örbom A, Altai M, et al. A conjugation strategy to modulate antigen binding and FcRn interaction leads to improved tumor targeting and radioimmunotherapy efficacy with an antibody targeting prostate-specific antigen. *Cancers (Basel).* 2021;13:3469.
11. Howe A, Bhatavdekar O, Salerno D, et al. Combination of carriers with complementary intratumoral microdistributions of delivered alpha-particles may realize the promise for ^{225}Ac in large, solid tumors. *J Nucl Med.* 2022;63:1223–1230.
12. Bernhardt P, Ahlman H, Forssell-Aronsson E. Model of metastatic growth valuable for radionuclide therapy. *Med Phys.* 2003;30:3227–3232.
13. Nahum AE. Microdosimetry and radiocurability: modelling targeted therapy with beta-emitters. *Phys Med Biol.* 1996;41:1957–1972.
14. Uusijärvi H, Bernhardt P, Forssell-Aronsson E. Tumour control probability (TCP) for non-uniform activity distribution in radionuclide therapy. *Phys Med Biol.* 2008; 53:4369–4381.
15. Falzone N, Lee BQ, Able S, et al. Targeting micrometastases: the effect of heterogeneous radionuclide distribution on tumor control probability. *J Nucl Med.* 2018; 60:250–258.
16. Sarrut D, Bardies M, Boussion N, et al. A review of the use and potential of the GATE Monte Carlo simulation code for radiation therapy and dosimetry applications. *Med Phys.* 2014;41:064301.
17. International Atomic Energy Agency. *LiveChart of Nuclides*. https://www-nds.iaea.org/relnsd/vcharthtml/VChartHTML.html (accessed July 2023).
18. Mougeot X. Towards high-precision calculation of electron capture decays. *Appl Radiat Isot.* 2019;154:108884.
19. Mougeot X. Erratum: reliability of usual assumptions in the calculation of beta and neutrino spectra [Phys. Rev. C 91, 055504 (2015)]. *Phys Rev C.* 2015;92:059902.
20. Berger MJ, Coursey JS, Zucker MA, Chang J. *ESTAR, PSTAR, and ASTAR: Computer Programs for Calculating Stopping-Power and Range Tables for Electrons, Protons, and Helium Ions.* National Institute of Standards and Technology; 2017.
21. Elgqvist J, Timmermand OV, Larsson E, Strand SE. Radiosensitivity of prostate cancer cell lines for irradiation from beta particle-emitting radionuclide ^{177}Lu compared to alpha particles and gamma rays. *Anticancer Res.* 2016;36:103–109.
22. Kristiansson A, Örbom A, Ahlstedt J, et al. ^{177}Lu-PSMA-617 therapy in mice, with or without the antioxidant $alpha_1$-microglobulin (A1M), including kidney damage assessment using ^{99m}Tc-MAG3 imaging. *Biomolecules.* 2021;11:263.
23. Sgouros G, Roeske JC, McDevitt MR, et al. MIRD pamphlet no. 22 (abridged): radiobiology and dosimetry of alpha-particle emitters for targeted radionuclide therapy. *J Nucl Med.* 2010;51:311–328.
24. Spoormans K, Crabbe M, Struelens L, De Saint-Hubert M, Koole M. A review on tumor control probability (TCP) and preclinical dosimetry in targeted radionuclide therapy (TRT). *Pharmaceutics.* 2022;14:2007.
25. Bordes J, Incerti S, Mora-Ramirez E, et al. Monte Carlo dosimetry of a realistic multicellular model of follicular lymphoma in a context of radioimmunotherapy. *Med Phys.* 2020;47:5222–5234.
26. Mínguez Gabiña P, Roeske JC, Mínguez R, Rodeño E, Gómez de Iturriaga A. Microdosimetry-based determination of tumour control probability curves for treatments with ^{225}Ac-PSMA of metastatic castration resistant prostate cancer. *Phys Med Biol.* 2020;65:235012.